Chapter 3

Scale Length Determination of Some Non-conventional Structures of JLT

3.1 Introduction

Switching speed of field effect devices has shown dramatic improvement over the past few decades, which is empowered by Silicon processing technology in conjunction with the continued device downscaling. Since the inception the MOS packaging density has undergone a two fold increase every 18 months as predicted by the Moore's law [1,2]. Reduction of physical dimension has not only improved circuit performance but also led to energy efficiency. The working frequency of a device increases with reduction in gate length. Actually the gate length or channel length determines the carrier transit time of the device. As the device area decreases, the overall gate capacitance also decreases. This results in faster switching of a device [3-6]. Consequently device scaling is a candid affair for performance improvement of a device.

Scale length is a representative parameter that gives an indication about the extent to which a device can be miniaturized. The scale length can be defined as the length of the portion of the channel that is under the control of drain [7-10]. The channel length of the device should be 5-10 times of the scale length to avoid short channel effect [6,10]. The scale length expression for the device is obtained by solving the Poisson's equation for transverse electrostatic potential [6]. In other words scale length value indicates the limit upto which a device can be scaled down. In this chapter methods for determination of scale length of four non conventional structures of JLT is presented. The structures are-

1. Pentagonal

2. Hexagonal

3. Octagonal

4. Rectangular

These structures have not been reported so far, probably because of the fabrication difficulties. As the fabrication technologies are developing rapidly, the possibility of fabrication of these structures in near future cannot be denied. Moreover the fabrication of

JLT is much simpler compared to devices with junctions [11-30]. So in this chapter a discussion is given on whether these structures are suitable for VLSI design by determining the scale length expressions for the above mentioned structures and comparing the scale length values for all the structures.

3.2 Scale Length Determination

The 3D Poisson's equation has been used to determine the scale length of the different structures of JLT. In some of the structures it is possible to convert the 3D Poisson's equation into a 2D equation. The boundary conditions for the Poisson's equation can be extracted for different structures which is dependent upon the geometric structure of the device. The 3D Poisson's equation can be written as [31],

$$\nabla^2\phi(x,y,z) = -\frac{\rho}{\in_{si}} = -\frac{q}{\in_{si}}(p - n + N_d - N_a) \tag{3.1}$$

Where,

$\phi(x,y,z)$ is the electrostatic potential

q is charge of a carrier (hole or electron),

N_a and N_d are the acceptor and donor doping concentrations

ϵ_{si} is the permittivity of silicon.

For P-channel device, n << p and $N_d << N_a$ and for N-channel device, p << n and $N_a << N_d$ [31]

Therefore equation (3.1) can be approximated as [31],

$$\nabla^2\phi(x,y,z) = -\frac{q}{\in_{si}}(p - N_a) = -\frac{q}{\in_{si}} N_a(e^{(-\frac{q\phi(x,y,z)}{kT})} - 1)$$ for P-channel JLT and

$$\nabla^2\phi(x,y,z) = \frac{q}{\in_{si}}(n - N_d) = \frac{q}{\in_{si}} N_d(e^{(-\frac{q\phi(x,y,z)}{kT})} - 1)$$ for N-channel JLT

Again, in the depletion region, p << N_a and n << N_d [31]

$$\phi(x,y,z) > 0 \Rightarrow e^{(-\frac{q\phi(x,y,z)}{kT})} \cong 0 \tag{3.2}$$

Using (3.2) , the Poisson's equation in the fully depleted channel can be written as [31],

$$\frac{\partial^2\phi(x,y,z)}{\partial x^2}+\frac{\partial^2\phi(x,y,z)}{\partial y^2}+\frac{\partial^2\phi(x,y,z)}{\partial z^2}=\frac{qN_a}{\in_{si}} \tag{3.3A}$$

for P-Channel JLT and

$$\frac{\partial^2\phi(x,y,z)}{\partial x^2}+\frac{\partial^2\phi(x,y,z)}{\partial y^2}+\frac{\partial^2\phi(x,y,z)}{\partial z^2}=-\frac{qN_d}{\in_{si}} \tag{3.3B}$$

for N-channel JLT

3.2.1 Pentagonal JLT

The schematic diagram of a pentagonal JLT is shown below in Fig. 3.1. The 3D Poisson's equation for a pentagonal JLT is presented as follows.

$$\frac{\partial^2\phi(x,y,z)}{\partial x^2}+\frac{\partial^2\phi(x,y,z)}{\partial y^2}+\frac{\partial^2\phi(x,y,z)}{\partial z^2}=\frac{qN_a}{\in_{si}} \tag{3.4A}$$

$$\frac{\partial^2\phi(x,y,z)}{\partial x^2}+\frac{\partial^2\phi(x,y,z)}{\partial y^2}+\frac{\partial^2\phi(x,y,z)}{\partial z^2}=-\frac{qN_d}{\in_{si}} \tag{3.4B}$$

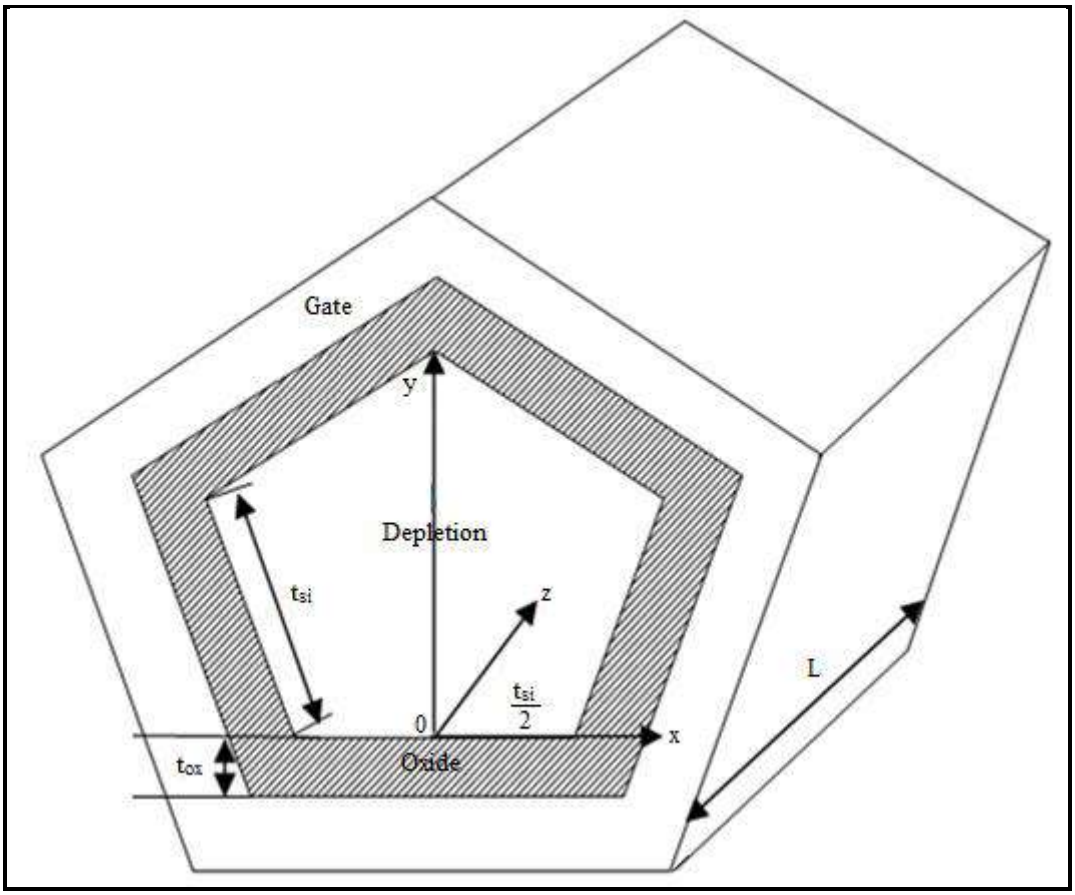

Fig. 3.1: Cross sectional view of a Gate all around (pentagonal cross section) JLT

A possible solution for (3.4) can be written as [32],

$$\phi(x,y,z) = C_0(z) + C_1(z)x + C_2(z)y + C_3(z)x^2 + C_4(z)y^2 \tag{3.5}$$

Cross sectional view of a Gate all around (pentagonal cross section) JLT in Fig. 3.1

For Full Depletion,

At $x = 0$, $y = 0$,

$$\phi(x,y,z) = C_0(z) = \phi_s$$

At $x = 0$, the electric field,

$$\frac{d\phi(x,y,z)}{dx} = C_1(z) = -\frac{\in_{ox}}{\in_{si} t_{ox}}(\phi_{gs} - \phi_s)$$

At $y = 0$, the electric field,

$$\frac{d\phi(x,y,z)}{dy} = C_2(z) = -\frac{\in_{ox}}{\in_{si} t_{ox}}(\phi_{gs} - \phi_s)$$

Where,

ϕ_s is the surface potential

ϵ_{ox} is the permittivity of the gate oxide

t_{ox} is the gate oxide thickness

$\phi_{gs} = V_{gs} - V_{fb}$

where,

V_{gs} is gate to source voltage

V_{fb} is the flat band voltage.

The distance of the centre of mass of the pentagon from the vertices is,

$$R = \frac{t_{si}}{2\sin 36^\circ} = \frac{t_{si}}{1.176}$$

Where,

t_{si} is the side length of the pentagon.

At $x=0$, $y=\frac{\sqrt{1-\sin^2 36^\circ}}{2\sin 36^\circ}t_{si}=0.69t_{si}$,

$$C_0(z)+C_2(z)0.69t_{si}+C_4(z)(0.69t_{si})^2=\phi_0(z)$$

$$C_4(z)=\frac{1}{(0.69t_{si})^2}(\phi_0(z)-\phi_s)+\frac{\in_{ox}}{0.69\in_{si} t_{ox}t_{si}}(\phi_{gs}-\phi_s)$$

At $y=0, x=\frac{1}{2}t_{si}$,

$$C_0(z)+C_1(z)\frac{t_{si}}{2}+C_3(z)(\frac{t_{si}}{2})^2=\phi_s$$

$$C_3(z)=\frac{2\in_{ox}}{\in_{si} t_{ox}t_{si}}(\phi_{gs}-\phi_s)$$

Therefore,

$$\phi(x,y,z)=\begin{aligned}&\phi_s-\frac{\in_{ox}}{\in_{si} t_{ox}}(\phi_{gs}-\phi_s)(x+y)+\frac{2\in_{ox}}{\in_{si} t_{ox}t_{si}}(\phi_{gs}-\phi_s)x^2+\\&[\frac{1}{(0.69t_{si})^2}(\phi_0(z)-\phi_s)+\frac{\in_{ox}}{0.69\in_{si} t_{ox}t_{si}}(\phi_{gs}-\phi_s)]y^2\end{aligned} \quad (3.6)$$

At $y=0, x=\frac{1}{2}t_{si}$,

$$\phi(x,y,z)=\phi_s=\phi_0(z)+\frac{\in_{ox}}{2t_{si}\in_{si} t_{ox}}(\phi_{gs}-\phi_s)t_{si}^2 \quad (3.7)$$

Using (3.7), (3.6) can also be written as,

$$\phi(x,y,z) = \phi_0(z)\frac{4.98t_{ox}\in_{si}}{4.98\in_{si} t_{ox}+1.9\in_{ox} t_{si}}+\frac{1.9\in_{ox} t_{si}}{4.98\in_{si} t_{ox}+1.9\in_{ox} t_{si}}\phi_{gs}-\frac{4.98t_{ox}\in_{si}}{4.98\in_{si} t_{ox}+1.9\in_{ox} t_{si}}(\phi_{gs}-\phi_0(z))(x+y)+\frac{9.96\in_{ox}}{t_{si}(4.98\in_{si} t_{ox}+1.9\in_{ox} t_{si})}(\phi_{gs}-\phi_0(z))x^2+\frac{11.3\in_{ox}}{t_{si}(4.98\in_{si} t_{ox}+1.9\in_{ox} t_{si})}(\phi_{gs}-\phi_0(z))y^2 \quad (3.8)$$

Putting $\phi(x,y,z)$ from (3.8) in (3.4) and $x=0$, $y=0.69t_{si}$,

Or, $$\frac{d^2\phi_0(z)}{dx^2}+\frac{1}{\lambda^2}(\phi_{gs}-\phi_0(z))=\frac{qN_a}{\in_{si}} \quad (3.9)$$

Where, $\lambda=\sqrt{\frac{t_{si}(4.98\in_{si} t_{ox}+1.9\in_{ox} t_{si})}{26.32\in_{ox}}}$ is the scale length of the device .

Solving (3.9) The central longitudinal potential can be obtained as [32],

$$\phi_0(z)=\frac{(V_{ds}+(\frac{qN_a}{\in_{si}}-\frac{1}{\lambda^2}\phi_{gs})\lambda^2)e^{\frac{L}{\lambda}}-(\frac{qN_a}{\in_{si}}-\frac{1}{\lambda^2}\phi_{gs})\lambda^2}{(e^{2\frac{L}{\lambda}}-1)}e^{\frac{z}{\lambda}}-\frac{(V_{ds}+(\frac{qN_a}{\in_{si}}-\frac{1}{\lambda^2}\phi_{gs})\lambda^2)e^{\frac{L}{\lambda}}-(\frac{qN_a}{\in_{si}}-\frac{1}{\lambda^2}\phi_{gs})\lambda^2 e^{2\frac{L}{\lambda}}}{(e^{2\frac{L}{\lambda}}-1)}e^{-\frac{z}{\lambda}}-(\frac{qN_a}{\in_{si}}-\frac{1}{\lambda^2}\phi_{gs})\lambda^2$$

3.2.2 Hexagonal JLT

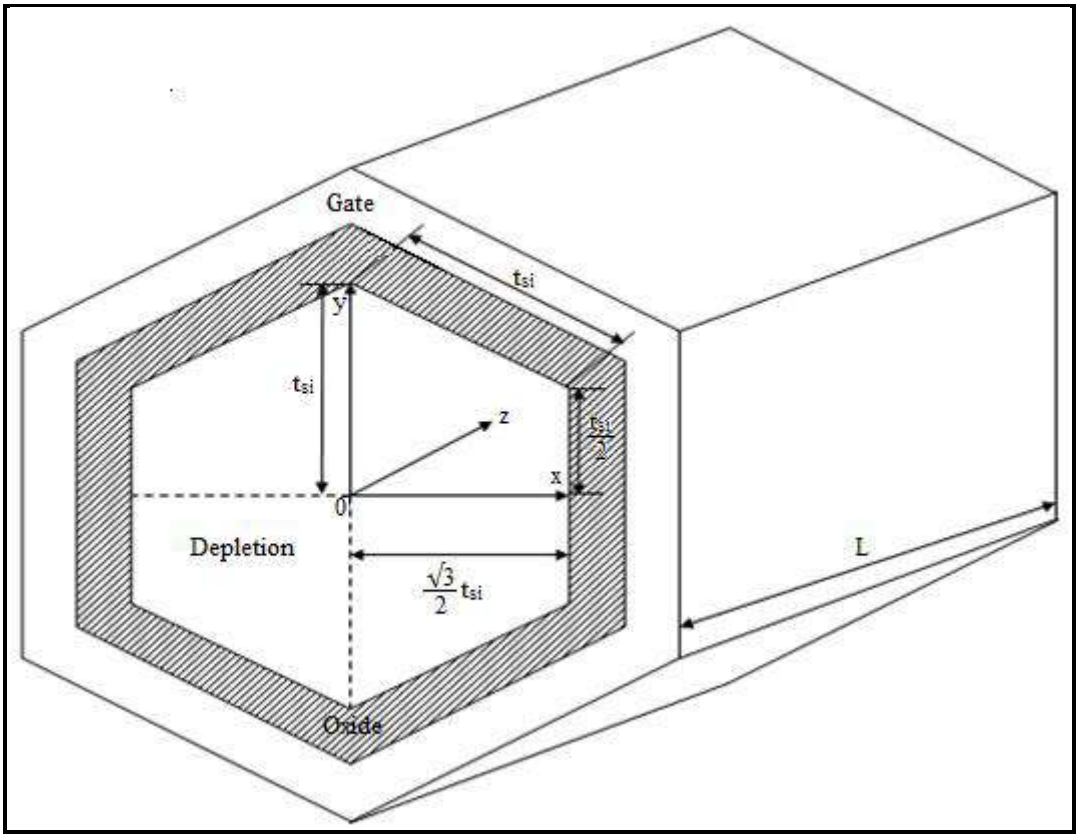

Fig. 3.2: Cross sectional view of a Gate all around (Hexagonal cross section) JLT

The schematic diagram of a hexagonal JLT is shown in Fig. 3.2.

For a n-type and p-type JLT the Poisson's equation in fully depleted channel is given below

$$\frac{\partial^2\phi(x,y,z)}{\partial x^2}+\frac{\partial^2\phi(x,y,z)}{\partial y^2}+\frac{\partial^2\phi(x,y,z)}{\partial z^2}=\frac{qN_a}{\in_{si}} \tag{3.10A}$$

$$\frac{\partial^2\phi(x,y,z)}{\partial x^2}+\frac{\partial^2\phi(x,y,z)}{\partial y^2}+\frac{\partial^2\phi(x,y,z)}{\partial z^2}=-\frac{qN_d}{\in_{si}} \tag{3.10B}$$

The possible general solution obtained as from equation (3.10) is [32]

$$\phi(x,y,z) = C_0(z) + C_1(z)x + C_2(z)y + C_3(z)x^2 + C_4(z)y^2$$

Using boundary conditions,

At $x = 0$, $y = 0$, $\phi(x,y,z) = C_0(z) = \phi_0(z)$

At $x = 0$, $y = 0$, the electric field is given as,

$$\frac{d\phi(x,y,z)}{dx} = \frac{d\phi(x,y,z)}{dy} = C_1(z) = C_2(z) = 0$$

At $x = \frac{\sqrt{3}}{2}t_{si}$, $y = 0$, the electric field is given as,

$$\frac{d\phi(x,y,z)}{dx} = \sqrt{3}t_{si}C_3(z) = \frac{\in_{ox}}{\in_{si} t_{ox}}(\phi_{gs} - \phi_s)$$

Or, $C_3(z) = \frac{\in_{ox}}{\sqrt{3}t_{si} \in_{si} t_{ox}}(\phi_{gs} - \phi_s)$

At $x = 0$, $y = t_{si}$, the electric field is given as,

$$\frac{d\phi(x,y,z)}{dy} = 2t_{si}C_4(z) = \frac{\in_{ox}}{\in_{si} t_{ox}}(\phi_{gs} - \phi_s)$$

Or, $C_4(z) = \frac{\in_{ox}}{2t_{si} \in_{si} t_{ox}}(\phi_{gs} - \phi_s)$

Therefore,

$$\phi(x,y,z)=\phi_0(z)+\frac{\in_{ox}}{\sqrt{3}t_{si}\in_{si}t_{ox}}(\phi_{gs}-\phi_s)x^2+\frac{\in_{ox}}{2t_{si}\in_{si}t_{ox}}(\phi_{gs}-\phi_s)y^2 \tag{3.11}$$

At $x=0$, $y=t_{Si}$, $\phi(x,y,z)=\phi_s=\phi_0(z)+\frac{\in_{ox}}{2t_{si}\in_{si}t_{ox}}(\phi_{gs}-\phi_s)t_{si}^{\,2}$ (3.12)

Putting ϕ_s from (3.12) in (3.11),

$$\phi(x,y,z)=\phi_0(z)+\frac{2\in_{ox}}{\sqrt{3}t_{si}(2t_{ox}\in_{si}+\in_{ox}t_{si})}(\phi_{gs}-\phi_0(z))x^2 + \frac{\in_{ox}}{t_{si}(2t_{ox}\in_{si}+\in_{ox}t_{si})}(\phi_{gs}-\phi_0(z))y^2 \tag{3.13}$$

Putting $\phi(x,y,z)$ from (3.13) in (3.10) and $y=0$

Or $\frac{d^2\phi_0(z)}{dz^2}+\frac{1}{\lambda^2}(\phi_{gs}-\phi_0(z))=\frac{qN_a}{\in_{si}}$ (3.14)

Where, $\lambda=\sqrt{\frac{\sqrt{3}t_{si}(2t_{ox}\in_{si}+\in_{ox}t_{si})}{(4+2\sqrt{3})\in_{ox}}}$ is the scale length of the device .

By solving (3.14) central potential can be obtained as [32]

$$\phi_0(z)=\frac{(V_{ds}+(\frac{qN_a}{\in_{si}}-\frac{1}{\lambda^2}\phi_{gs})\lambda^2)e^{\frac{L}{\lambda}}-(\frac{qN_a}{\in_{si}}-\frac{1}{\lambda^2}\phi_{gs})\lambda^2}{(e^{2\frac{L}{\lambda}}-1)}e^{\frac{z}{\lambda}}- \frac{(V_{ds}+(\frac{qN_a}{\in_{si}}-\frac{1}{\lambda^2}\phi_{gs})\lambda^2)e^{\frac{L}{\lambda}}-(\frac{qN_a}{\in_{si}}-\frac{1}{\lambda^2}\phi_{gs})\lambda^2e^{2\frac{L}{\lambda}}}{(e^{2\frac{L}{\lambda}}-1)}e^{-\frac{z}{\lambda}}-(\frac{qN_a}{\in_{si}}-\frac{1}{\lambda^2}\phi_{gs})\lambda^2$$

3.2.3 Octagonal JLT

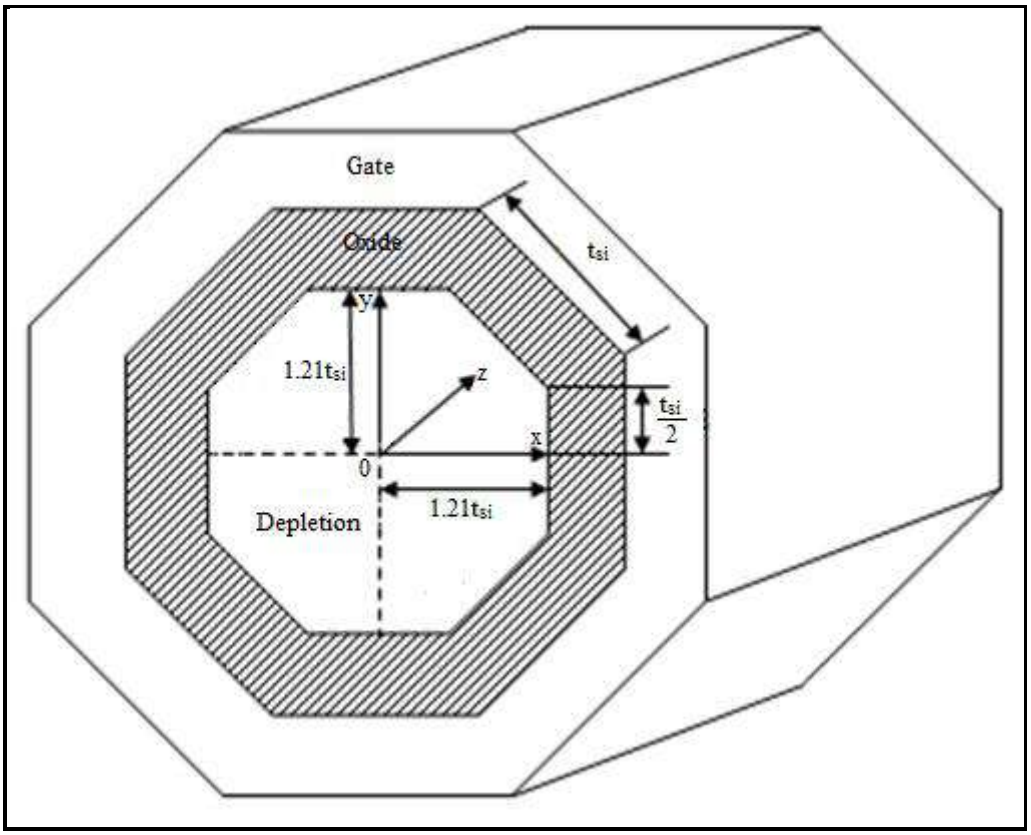

Fig. 3.3: Cross sectional view of a Gate all around (Octagonal cross section) JLT

In an octagonal JLT shown in Fig. 3.3 the origin of the coordinate system used is equidistant from all the sides. Therefore we can convert the 3D Poisson's equation into 2D equation as shown in equation (3.15).

Equation (3.3) for Gate all around (octagonal cross section) JLT can be rewritten as,

$$2\frac{\partial^2\phi(y,z)}{\partial y^2}+\frac{\partial^2\phi(y,z)}{\partial z^2}=\frac{qN_a}{\in_{si}} \tag{3.15}$$

One solution of Poisson's equation can be assumed as [32]

$$\phi(y,z) = C_0(z) + C_1(z)y + C_2(z)y^2 \tag{3.16}$$

At y=0,

$$\phi(y,z) = C_0(z) = \phi_0(z)$$

$\phi_0(z)$ is the central electrostatic potential.

At y=0, the transverse electric field in y- direction,

$$\frac{d\phi(y,z)}{dy} = C_1(z) = 0$$

At y=1.21t_{si}, where, t_{si} is the side length of octagon the electric field is given as,

$$\frac{d\phi(y,z)}{dy} = 2.42t_{si}C_2(z) = \frac{\in_{ox}}{\in_{si} t_{ox}}(\phi_{gs} - \phi_s)$$

Or $$\frac{d\phi(y,z)}{dy} = C_2(z) = \frac{\in_{ox}}{2.42t_{si} \in_{si} t_{ox}}(\phi_{gs} - \phi_s)$$

Therefore,

$$\phi(y,z) = \phi_0(z) + \frac{\in_{ox}}{2.42t_{si} \in_{si} t_{ox}}(\phi_{gs} - \phi_s)y^2 \tag{3.17}$$

(3.17) can also be written as,

$$\phi(y,z) = \phi_0(z) + \frac{\in_{ox}}{2.42t_{si}(\in_{si} t_{ox} + 0.6t_{si} \in_{ox})}(\phi_{gs} - \phi_0(z))y^2 \tag{3.18}$$

Putting $\phi(y,z)$ from (3.18) in (3.16) and y=0,

$$\frac{d^2\phi_0(z)}{dz^2}+\frac{1}{\lambda^2}(\phi_{gs}-\phi_0(z))=\frac{qN_a}{\in_{si}} \tag{3.19}$$

Where,

$\lambda=\sqrt{\frac{2.42t_{si}(t_{ox}\in_{si}+0.6\in_{ox}t_{si})}{4\in_{ox}}}$ is the scale length of the device.

By solving (3.19) central potential can be obtained as [32]

$$\phi_0(z)=\frac{(V_{ds}+(\frac{qN_a}{\in_{si}}-\frac{1}{\lambda^2}\phi_{gs})\lambda^2)e^{\frac{L}{\lambda}}-(\frac{qN_a}{\in_{si}}-\frac{1}{\lambda^2}\phi_{gs})\lambda^2}{(e^{2\frac{L}{\lambda}}-1)}e^{\frac{z}{\lambda}}-$$
$$\frac{(V_{ds}+(\frac{qN_a}{\in_{si}}-\frac{1}{\lambda^2}\phi_{gs})\lambda^2)e^{\frac{L}{\lambda}}-(\frac{qN_a}{\in_{si}}-\frac{1}{\lambda^2}\phi_{gs})\lambda^2e^{2\frac{L}{\lambda}}}{(e^{2\frac{L}{\lambda}}-1)}e^{-\frac{z}{\lambda}}-(\frac{qN_a}{\in_{si}}-\frac{1}{\lambda^2}\phi_{gs})\lambda^2$$

3.2.4 Rectangular JLT

The schematic diagram of rectangular JLT is shown in Fig. 3.4. The Poisson's equation can be written as,

$$\frac{\partial^2\phi(x,y,z)}{\partial x^2}+\frac{\partial^2\phi(x,y,z)}{\partial y^2}+\frac{\partial^2\phi(x,y,z)}{\partial z^2}=\frac{qN_a}{\in_{si}} \tag{3.20A}$$

$$\frac{\partial^2\phi(x,y,z)}{\partial x^2}+\frac{\partial^2\phi(x,y,z)}{\partial y^2}+\frac{\partial^2\phi(x,y,z)}{\partial z^2}=-\frac{qN_d}{\in_{si}} \tag{3.20B}$$

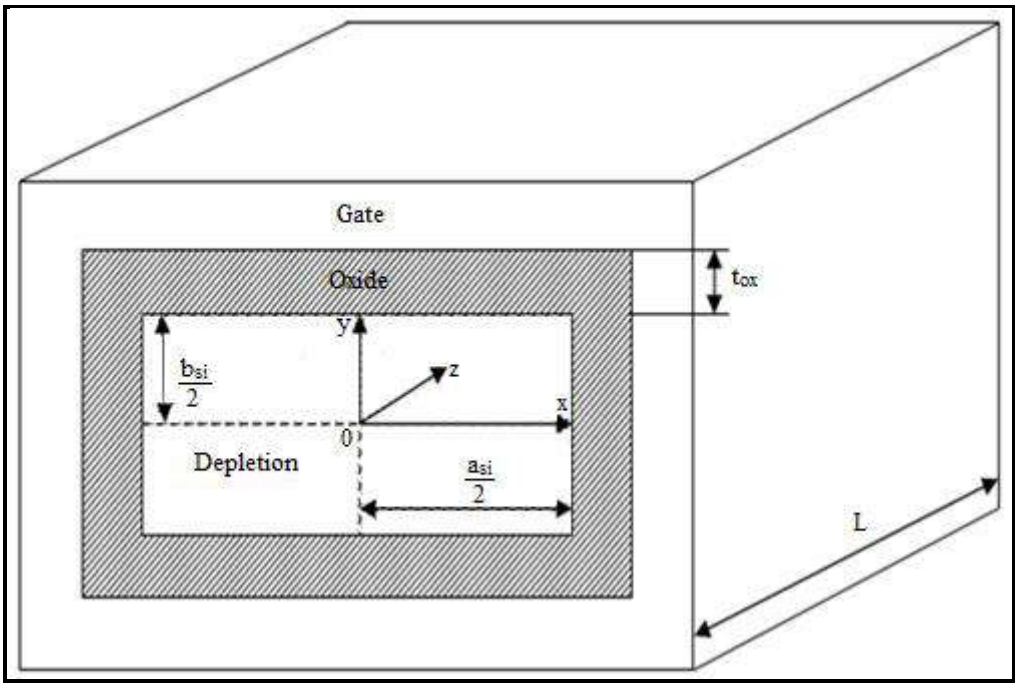

Fig. 3.4: Cross sectional view of a Gate all around (Rectangular cross section) JLT

The general solution of Poisson's equation can be obtained as [32]

$$\phi(x,y,z) = C_0(z) + C_1(z)x + C_2(z)y + C_3(z)x^2 + C_4(z)y^2$$

At x=0, y=0, $\phi(x,y,z) = C_0(z) = \phi_0(z)$ and

$$\frac{d\phi(x,y,z)}{dx} = \frac{d\phi(x,y,z)}{dy} = C_1(z) = C_2(z) = 0$$

Where, $\phi_0(z)$ is the central electrostatic potential.

At $x = \frac{a_{si}}{2}$, the transverse electric field in x-direction,

$$\frac{d\phi(x,y,z)}{dx} = a_{si}C_3(z) = \frac{\in_{ox}}{\in_{si} t_{ox}}(\phi_{gs} - \phi_s)$$

Or, $C_3(z) = \frac{\in_{ox}}{a_{si} \in_{si} t_{ox}}(\phi_{gs} - \phi_s)$

At $y = \frac{b_{si}}{2}$, the transverse electric field in y- direction ,

$$\frac{d\phi(x,y,z)}{dy} = b_{si}C_4(z) = \frac{\in_{ox}}{\in_{si} t_{ox}}(\phi_{gs} - \phi_s)$$

Or $C_4(z) = \frac{\in_{ox}}{b_{si} \in_{si} t_{ox}}(\phi_{gs} - \phi_s)$

Therefore (2) can be written as,

$$\phi(x,y,z) = \phi_0(z) + \frac{\in_{ox}}{a_{si} \in_{si} t_{ox}}(\phi_{gs} - \phi_s)x^2 + \frac{\in_{ox}}{b_{si} \in_{si} t_{ox}}(\phi_{gs} - \phi_s)y^2 \quad (3.21)$$

(3.21) can also be written as,

$$\phi(x,y,z) = \phi_0(z) + \frac{4 \in_{ox}}{a_{si}(4 \in_{si} t_{ox} + \in_{ox} a_{si} + \in_{ox} b_{si})}(\phi_{gs} - \phi_0(z))x^2 + \frac{4 \in_{ox}}{b_{si}(4 \in_{si} t_{ox} + \in_{ox} a_{si} + \in_{ox} b_{si})}(\phi_{gs} - \phi_0(z))y^2 \quad (3.22)$$

Putting $\phi(x,y,z)$ from (3.22) in (3.20) and x=0, y=0,

$$\frac{d^2\phi_0(z)}{dz^2} + \frac{1}{\lambda^2}(\phi_{gs} - \phi_0(z)) = \frac{qN_a}{\in_{si}} \quad (3.23)$$

Where,

$\lambda = \sqrt{\frac{a_{si} b_{si} (4t_{ox} \in_{si} + \in_{ox} a_{si} + \in_{ox} b_{si})}{8 \in_{ox} (a_{si} + b_{si})}}$ is the scale length of the device.

By solving (3.23) the central electrostatic potential can be determined as [32],

$$\phi_0(z) = \frac{(V_{ds} + (\frac{qN_a}{\in_{si}} - \frac{1}{\lambda^2}\phi_{gs})\lambda^2)e^{\frac{L}{\lambda}} - (\frac{qN_a}{\in_{si}} - \frac{1}{\lambda^2}\phi_{gs})\lambda^2}{(e^{2\frac{L}{\lambda}} - 1)} e^{\frac{z}{\lambda}} -$$

$$\frac{(V_{ds} + (\frac{qN_a}{\in_{si}} - \frac{1}{\lambda^2}\phi_{gs})\lambda^2)e^{\frac{L}{\lambda}} - (\frac{qN_a}{\in_{si}} - \frac{1}{\lambda^2}\phi_{gs})\lambda^2 e^{2\frac{L}{\lambda}}}{(e^{2\frac{L}{\lambda}} - 1)} e^{-\frac{z}{\lambda}} - (\frac{qN_a}{\in_{si}} - \frac{1}{\lambda^2}\phi_{gs})\lambda^2$$

3.3 Results And Discussion

A comparison of scale length variation with gate oxide thickness for the structures of JLT is shown in Fig. 3.5 and the variation of scale length with side lengths of the structures is shown in Fig. 3.6. The width to thickness ratio of the rectangular JLT is taken as 1. In Fig. 3.7 the variation of scale length of the rectangular JLT with width to thickness ratio cross section keeping the area constant (100 nm²) is shown. The scale length decreases nonlinearly with increasing width to thickness ratio. The variation of scale length with dielectric constant of gate dielectric for all the structures of JLT is shown in Fig. 3.8. It can be seen that to reduce channel length the gate oxide thickness should be decreased as capacitive coupling is higher for lower gate oxide thickness. Use of high K dielectric also strengthen the capacitive coupling which can push the channel length scaling limit further as shown in Fig. 3.8. From Fig. 3.5, Fig. 3.6 and Fig. 3.8 it is seen that the scale is lowest for hexagonal structure. However with a very high width to thickness ratio a lower scale length value can be achieved for rectangular structure as shown in Fig. 3.7.

The transverse electrostatic potential profile for different values of drain voltage, gate oxide thickness, channel length and gate voltage are shown in Fig. 3.9-Fig. 3.12. The electrostatic potential with respect to y-axis position starting from midpoint of one side to the midpoint of opposite side is plotted with origin at the centre. The central potential profile for different values of drain voltage, gate oxide thickness and gate voltage, are shown in Fig. 3.13-Fig. 3.15. The potential along channel length at the centre is plotted with position from source to drain. In the source end the potential is ideally zero which decreases initially and then increases and become equals to drain voltage at the drain end of the channel.

With the increasing drain voltage the gate control over the channel decreases and variation of potential increases. This is because the electric field due to drain voltage opposes the applied gate electric field. As the oxide thickness increases the vertical electric field reduces causing a decrease in the potential value. For shorter channel bending degree is high, which implies that the DIBL is more significant for the shorter device. As gate voltage increases the resultant electric field in the channel reduces causing the potential to reduce. In all cases the hexagonal structure exhibits minimum potential as the gate controllability is maximum for hexagonal JLT.

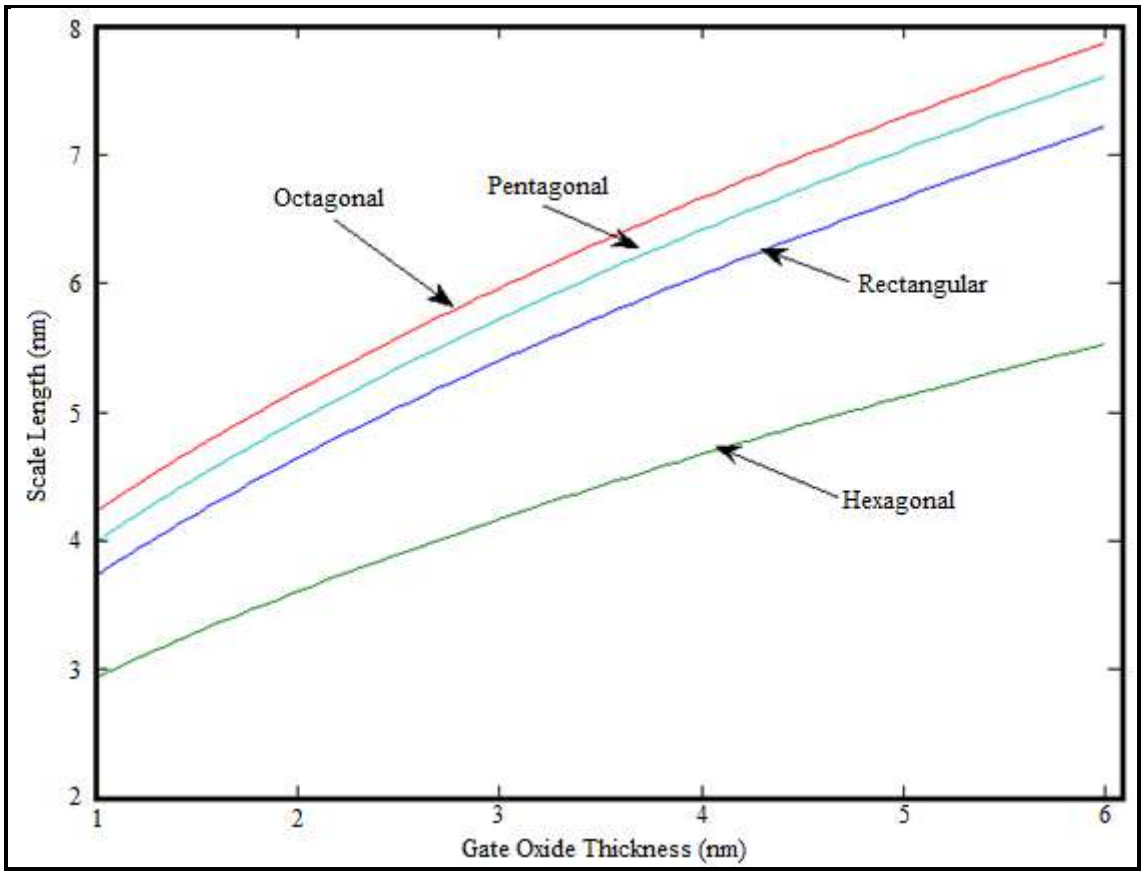

Fig. 3.5: Scale length variation with gate oxide thickness

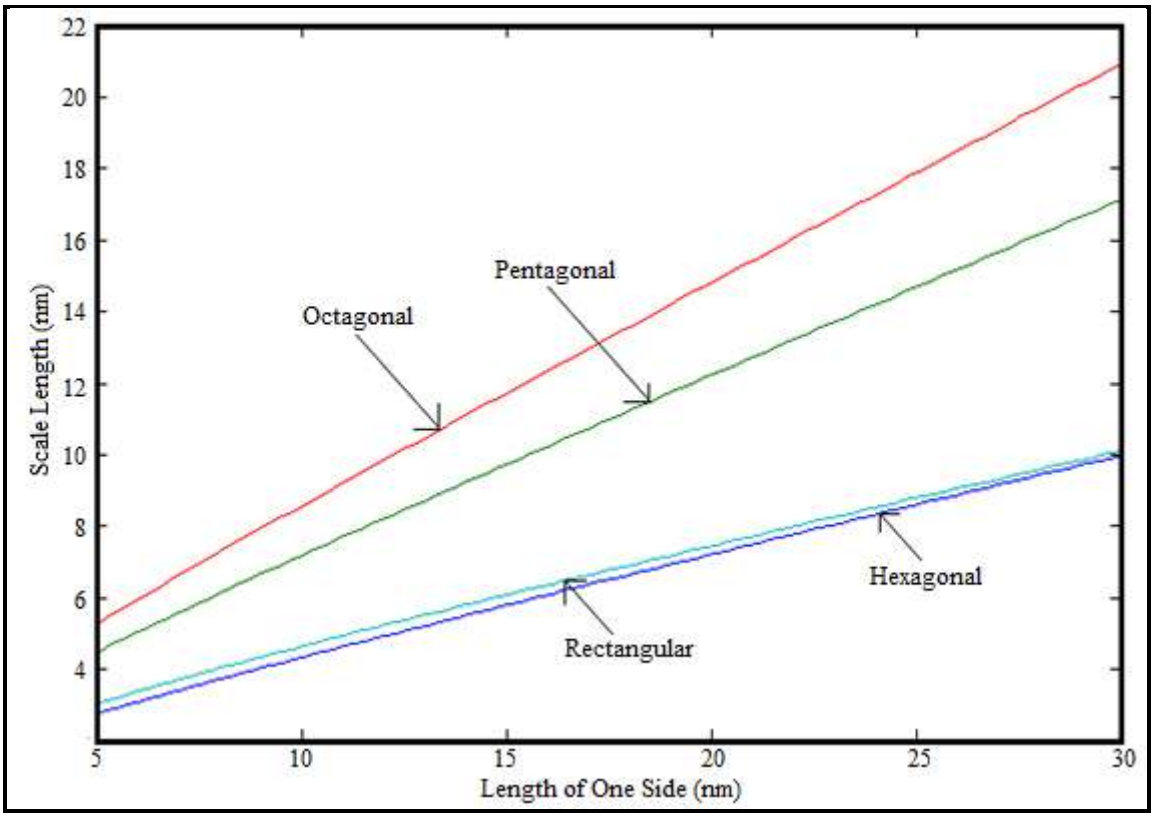

Fig. 3.6: Scale length variation with side length

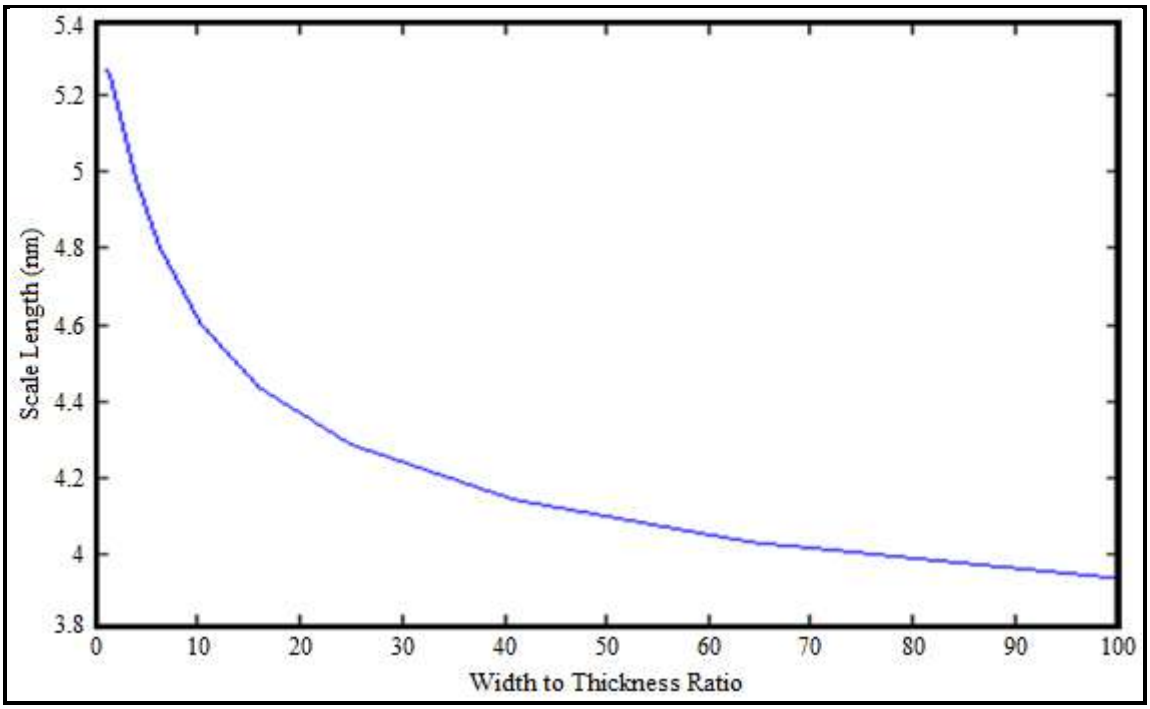

Fig. 3.7: Scale length variation with width to thickness ratio rectangular JLT keeping constant cross sectional area

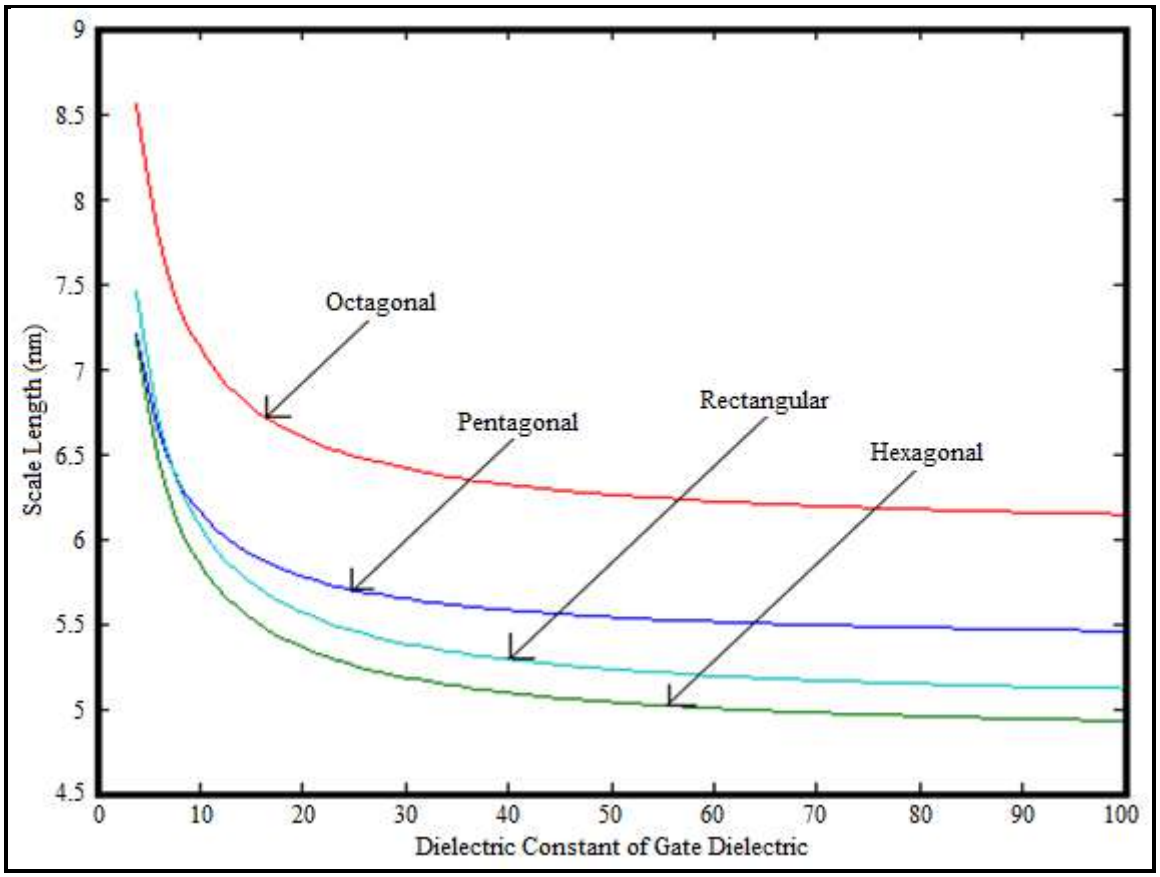

Fig. 3.8: Scale length variation with dielectric constant of gate dielectric

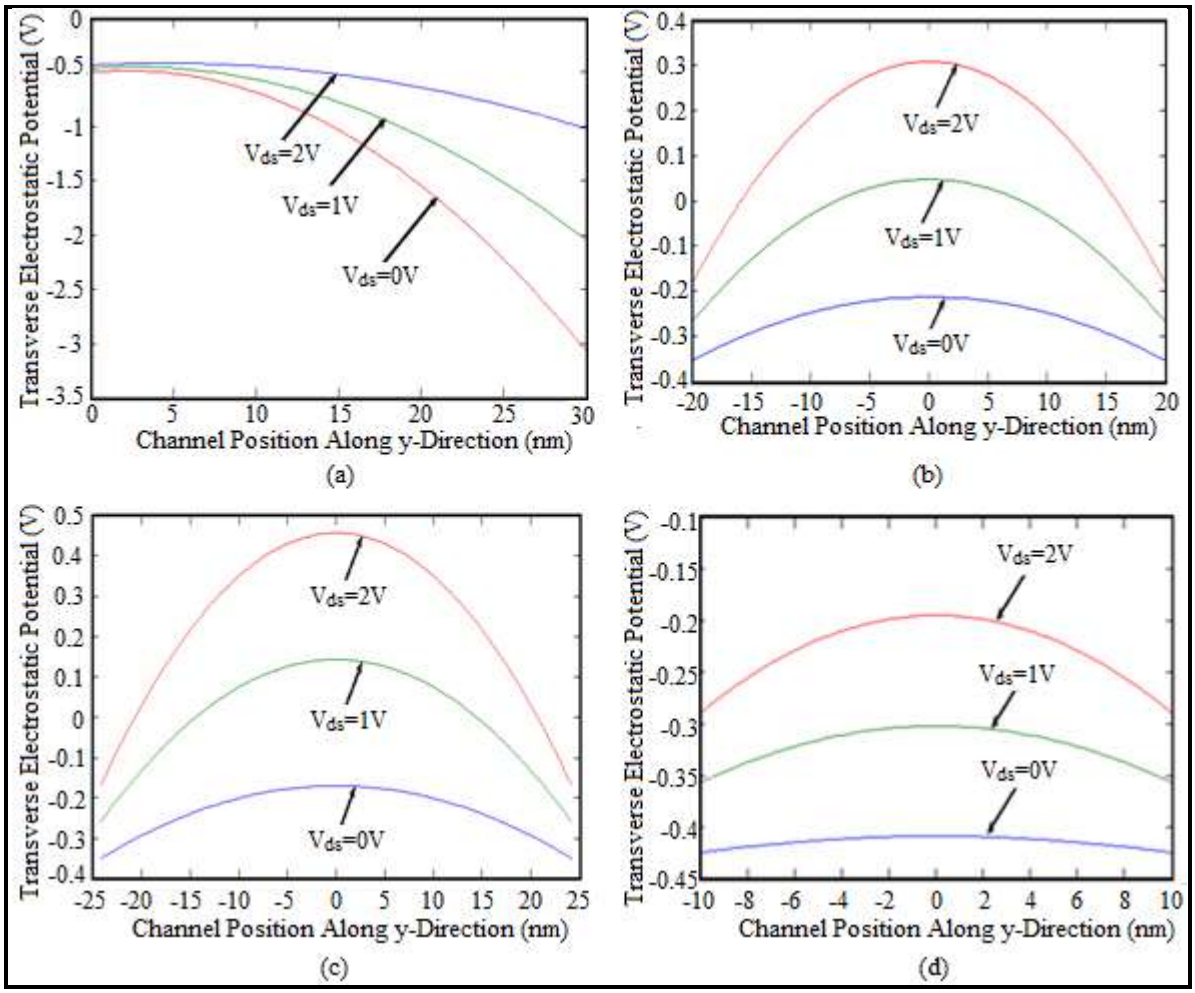

Fig. 3.9: Transverse potential profile for different value of drain to source voltage for (a) Pentagonal (b) Hexagonal (c) Octagonal (d) Rectangular JLT

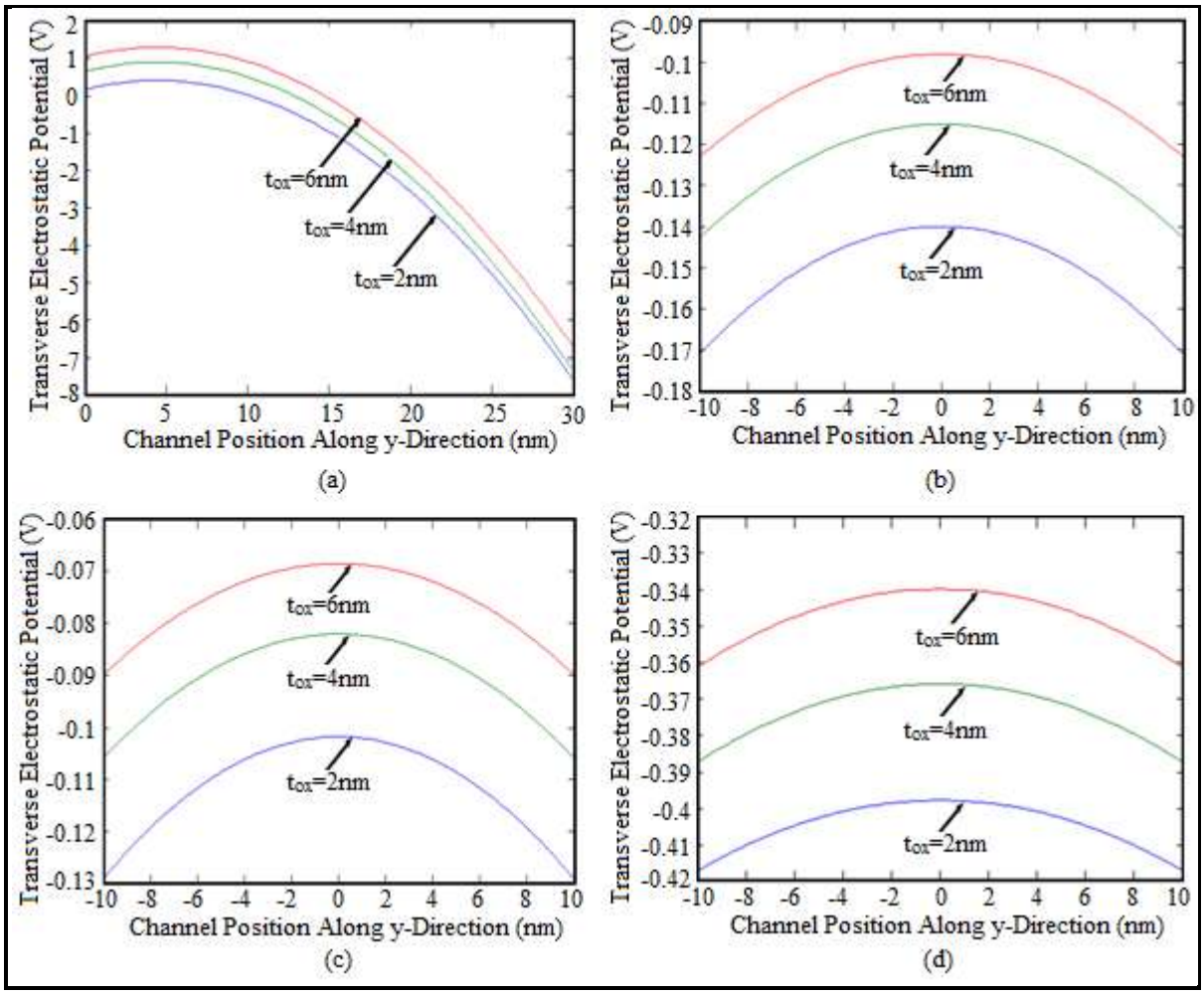

Fig. 3.10: Transverse potential profile for different value of gate oxide thickness for (a) Pentagonal (b) Hexagonal (c) Octagonal (d) Rectangular JLT

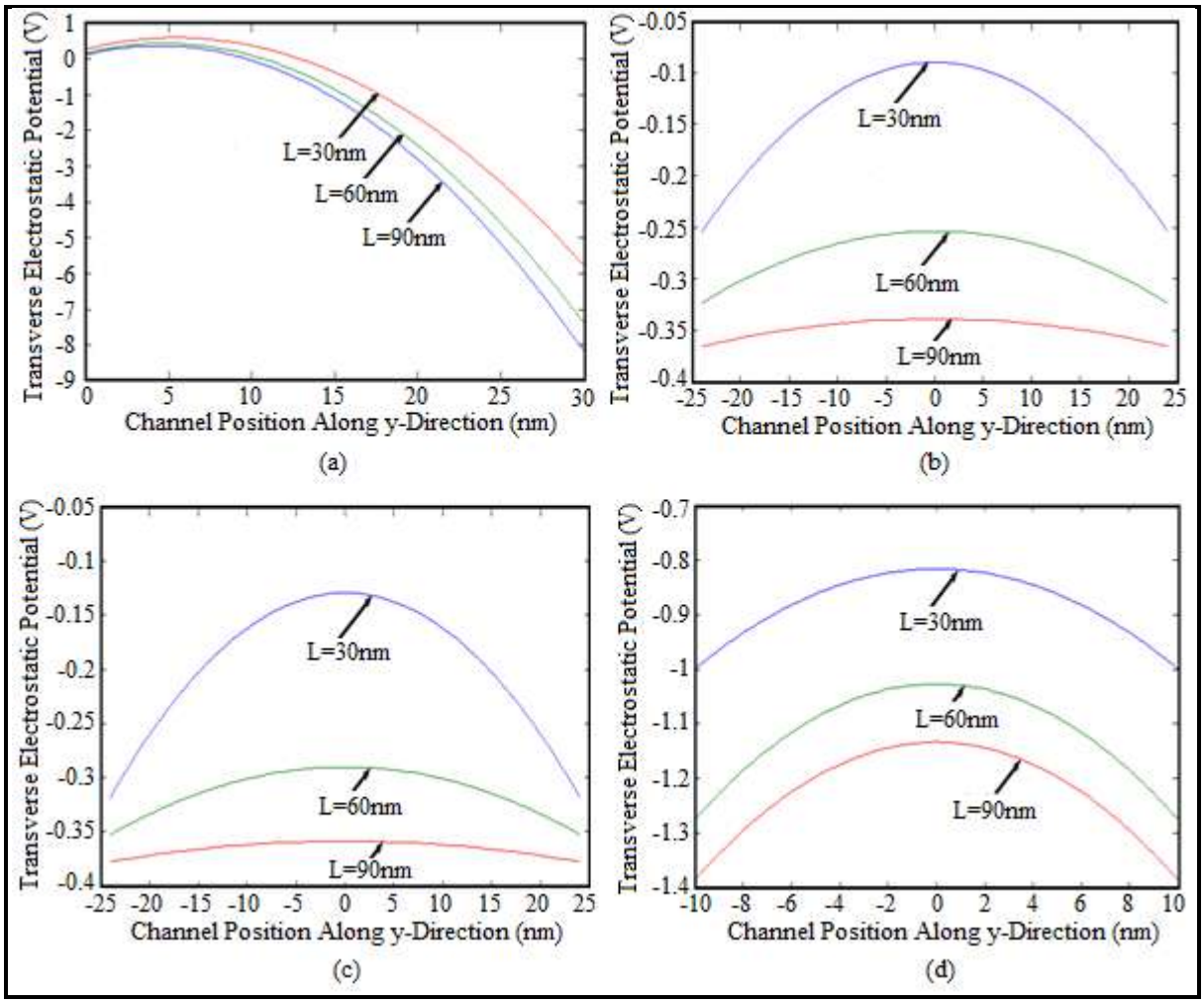

Fig. 3.11: Transverse potential profile for different value of channel length for (a) Pentagonal (b) Hexagonal (c) Octagonal (d) Rectangular JLT

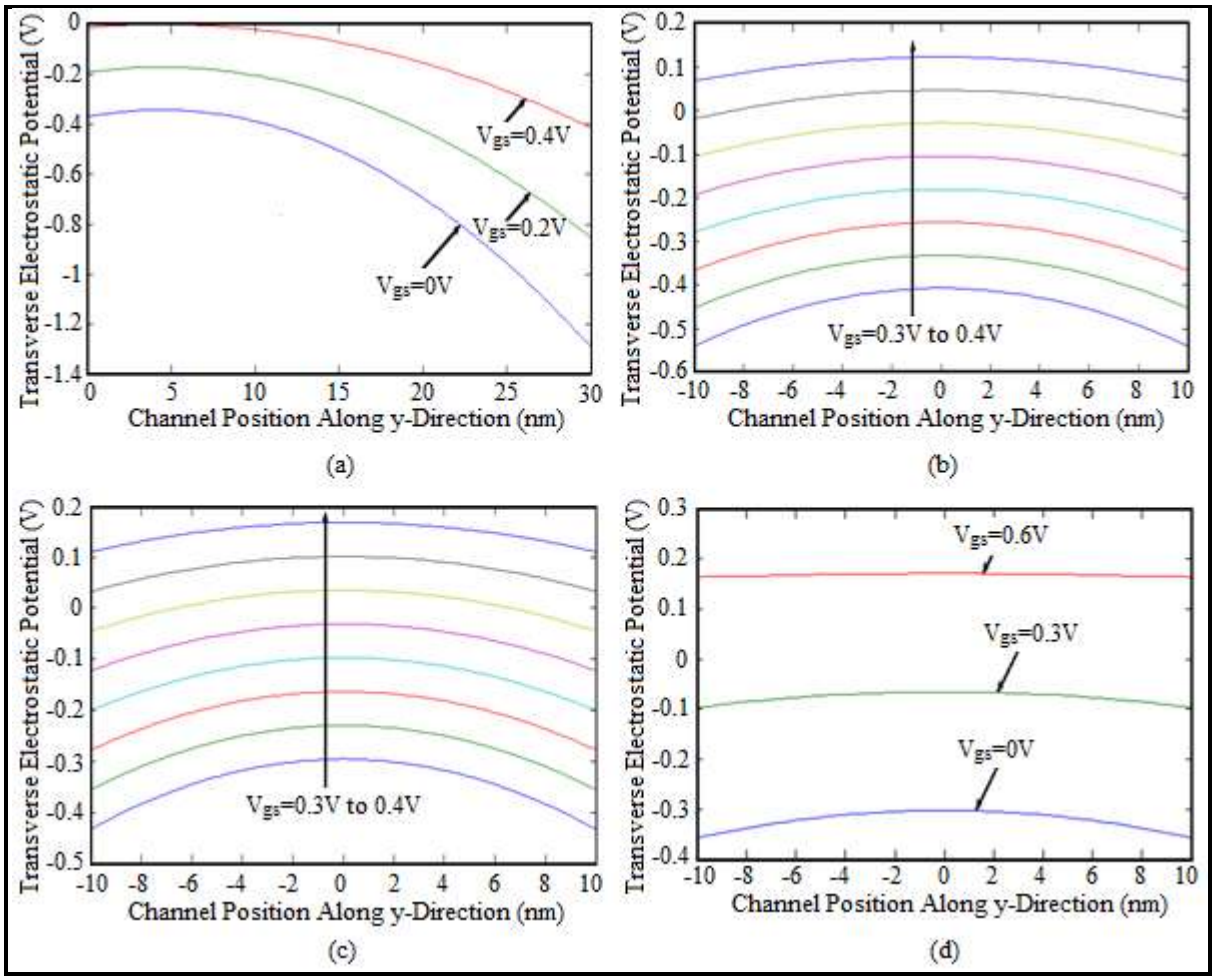

Fig. 3.12: Transverse potential profile for different value of gate to source voltage for (a) Pentagonal (b) Hexagonal (c) Octagonal (d) Rectangular JLT

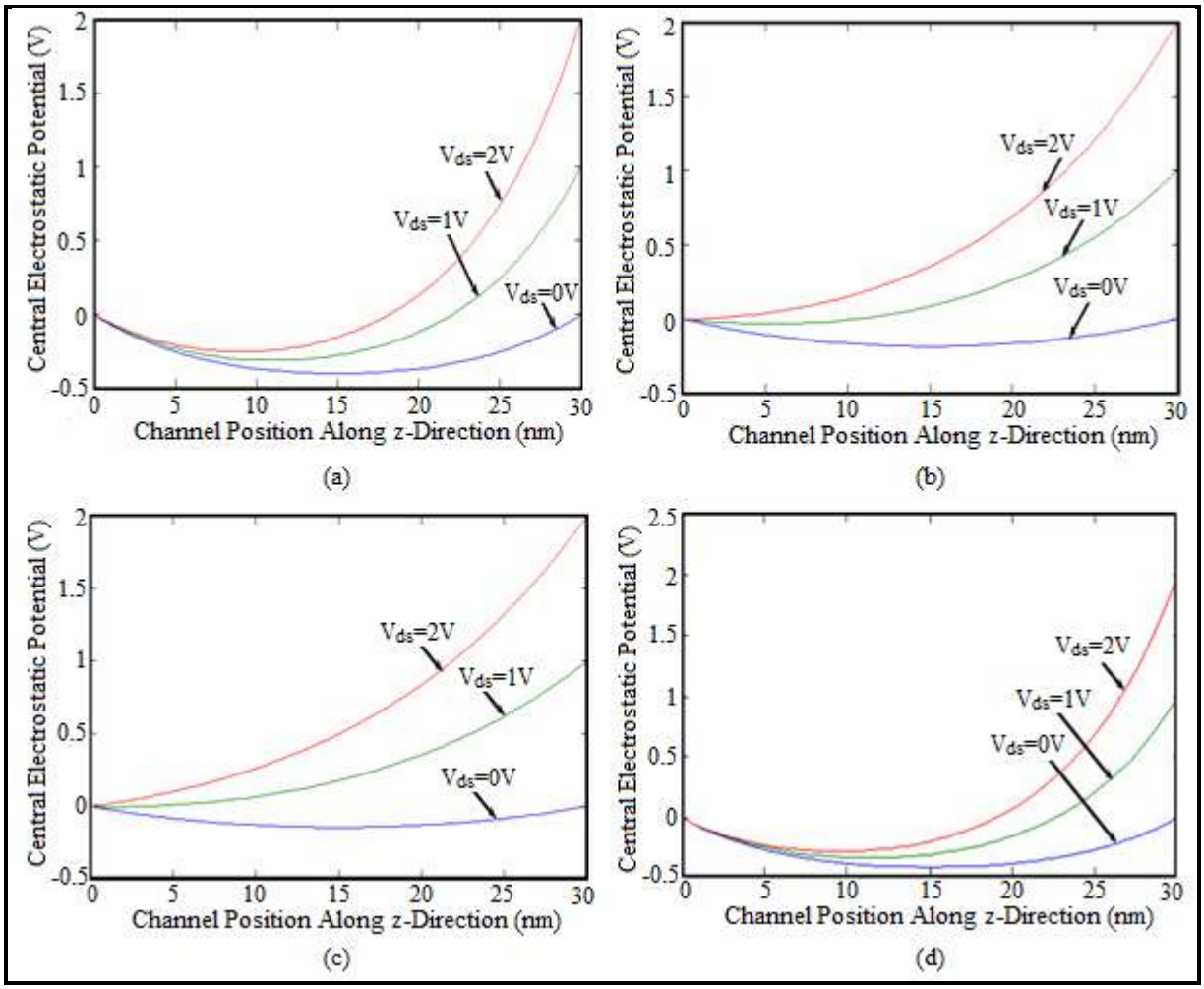

Fig. 3.13: Central potential profile for different value of drain to source voltage for (a) Pentagonal (b) Hexagonal (c) Octagonal (d) Rectangular JLT

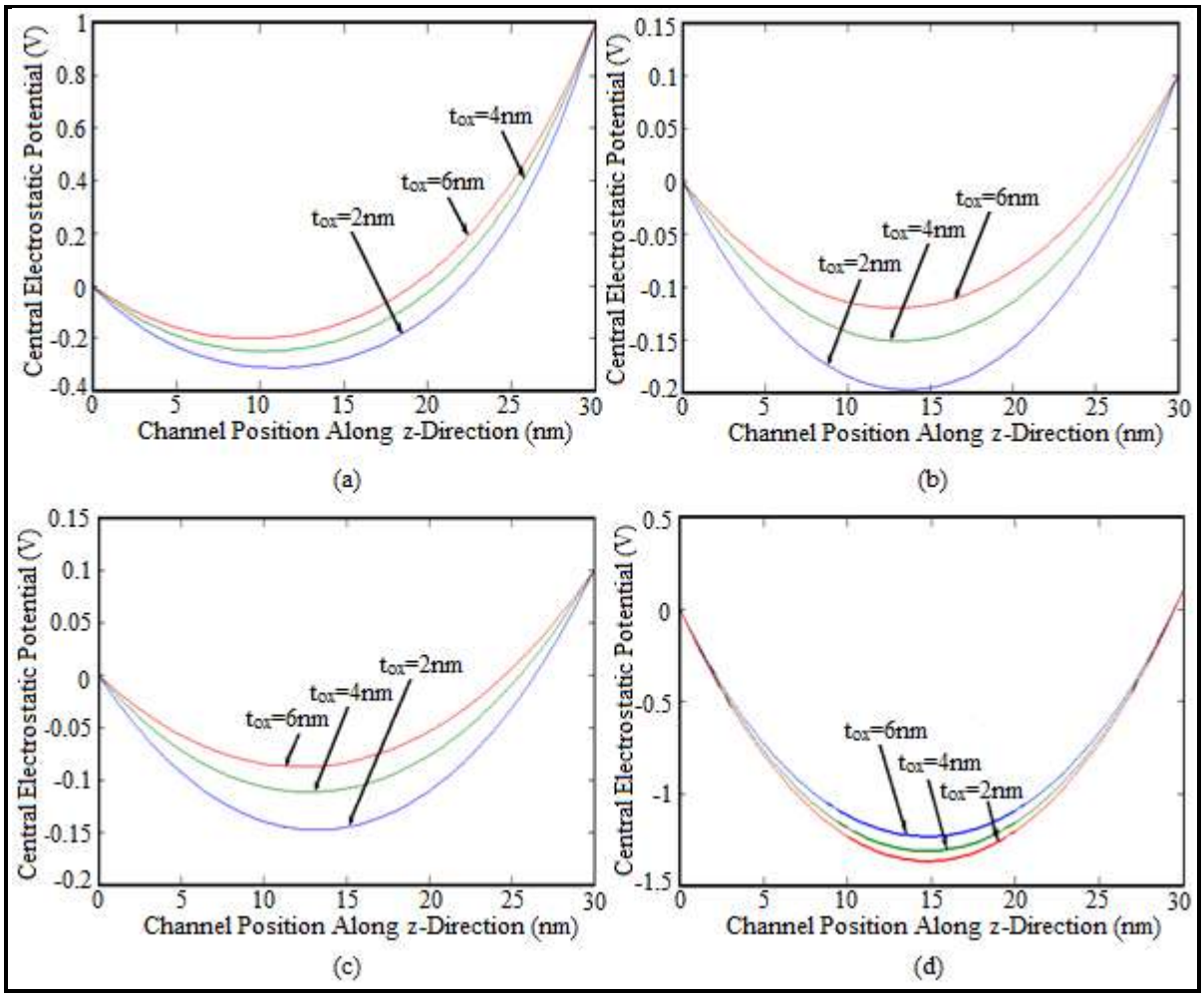

Fig. 3.14: Central potential profile for different value of gate oxide thickness for (a) Pentagonal (b) Hexagonal (c) Octagonal (d) Rectangular JLT

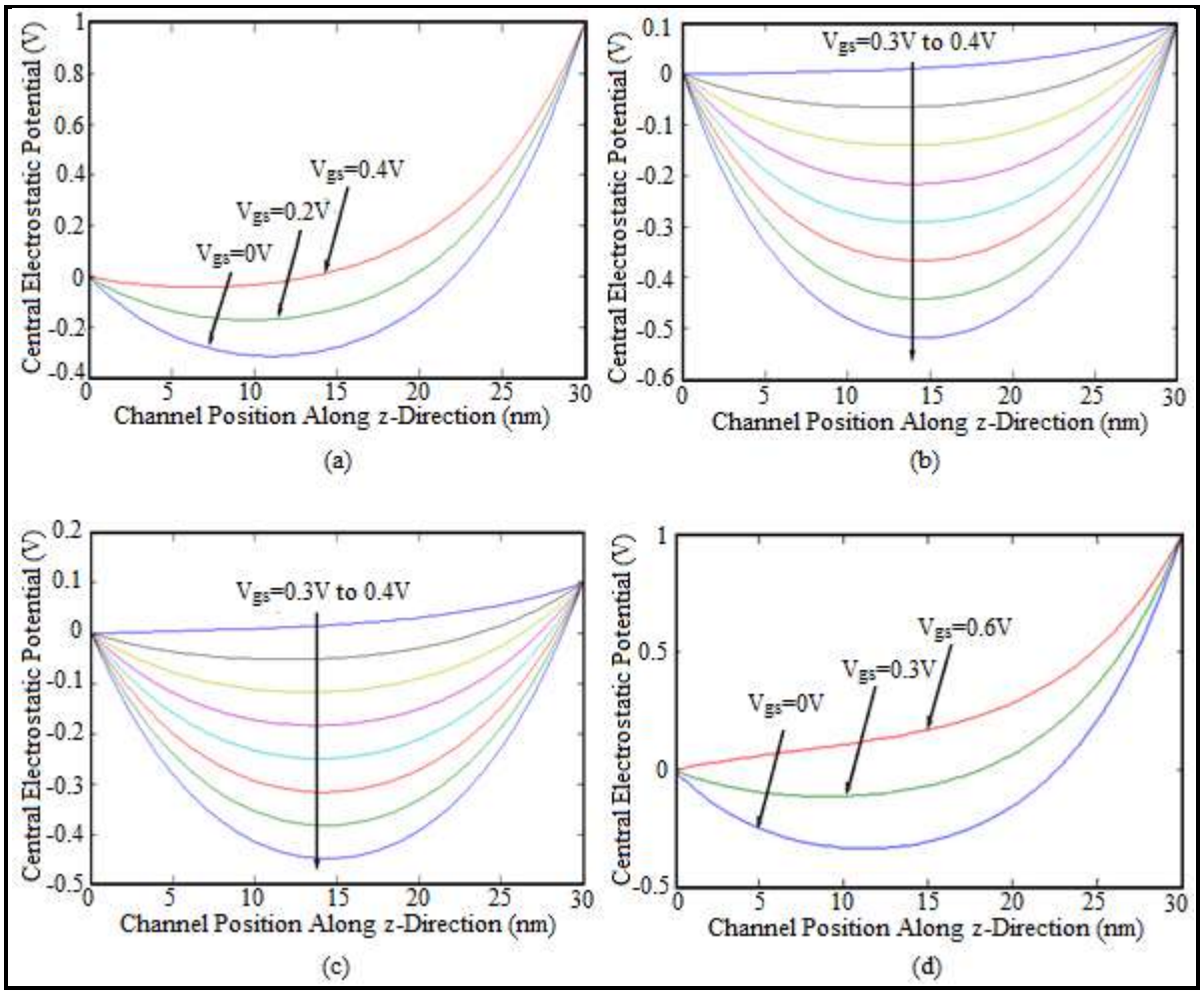

Fig. 3.15: Central potential profile for different value of gate to source voltage for (a) Pentagonal (b) Hexagonal (c) Octagonal (d) Rectangular JLT

3.4 Conclusions

The scale length expression for four structures of JLT namely pentagonal, hexagonal, octagonal and rectangular is obtained. Among the structures mentioned above the hexagonal and rectangular structures have the maximum packing density. The scale length value of hexagonal JLT is lowest among the structures. However for a very high width to thickness ratio the scale length value of rectangular JLT is less than the hexagonal JLT. Thus the hexagonal or rectangular or both structure may find their use in VLSI design in future.

Contributions

This chapter gives an idea about the scaling limit of the four structures mentioned. With the knowledge of the scaling limit along with some other characteristics such as, switching speed, power consumption etc. one can select the appropriate structure for a particular design.

Bibliography:

[1] Moore, G. E. Cramming More Components onto Integrated Circuits. *Electronics Magazine*, 38(8), April 19, 1965

[2] Moore, G. E. Progress in Digital Integrated Electronics. *IEDM Technical Digest*, IEEE press, pages 11-13, 1975

[3] Taur, Y. and Ning, T. H. *Fundamentals of Modern VLSI Devices*, Cambridge University Press, 1998

[4] Baccarani, G., Wordeman, M. R. and Dennard, R. H. Generalised Scaling Theory and its Application to ¼ Micrometer MOSFET Design. *IEEE Transactions on Electron Devices*, 31(4), pages 452-462, 1984

[5] Novak, E. J. Maintaining The Benefits of CMOS Scaling When Scaling Bogs Down. *IBM Journal of Research and Development*, 46, pages 169-180, 2002

[6] Colinge, J. P. Multiple-gate SOI MOSFETs. *Solid-State Electronics* 48, 897–905, 2004

[7] Yan, R. H. Ourmazd A. and Lee K. F. Scaling the Si MOSFET: From Bulk to SOI to Bulk. *IEEE Transactions on Electron Devices*, 39(7), pages 1704-1710, 1992

[8] Auth, C. P. Plummer J. D. Scaling Theory for Cylindrical, Fully-Depleted, Surrounding-Gate MOSFETs. *IEEE Electron Device Letters* 18(2), pages 74-76, 1997

[9] Colinge, J. P. The New Generation of SOI MOSFETs. *Romanian Journal of Information Science and Technology*, 11(1), pages 3-15, 2008

[10] Liu, Z. H., Hu, C., Huang, J. H., Chan, T. Y., Jeng, M. C., Ko, P. K. and Cheng, Y. C. Threshold Voltage Model for Deep-submicrometer MOSFETs. *IEEE Transactions on Electron Devices*, 40, pages 86-95, 1993.

[11] Colinge J. P., Lee, C. W., Afzalian, A., Dehdashti, N., Yan, R., Ferain, I., Razavi, P., O'Neill, B., Blake, A., White, M., Kelleher, A. M., McCarthy B., and Murphy R. SOI Gated Resistor: CMOS without Junctions. In *IEEE International SOI Conference*, pages 1-2, Foster City, California, USA , 2009

[12] Lee, C. W., Afzalian, A., Akhavan, N. D., Yan, R., Ferain, I., and Colinge. J. P. Junctionless Multigate Field Effect Transistor. *Applied Physics Letters*, 94(5), pages 053511, 2009

[13] Nazarov, A., Balestra, F., Raskin, J. P., Gamiz, F., and Lysenko, V. S. *Semiconductor-On-Insulator Materials for Nanoelectronics Applications*, Springer, 2011

[14] Gnani, E., Gnudi, A., Reggiani, S., and Baccarani, G. Theory of The Junctionless Nanowire FET. *IEEE Transactions on Electron Devices*, 58(9), pages 2903 - 2910, 2011

[15] Colinge, J. P., Lee, H. W., Afzalian, A., Akhavan, N. D., Yan, R., Ferain, I., Razavi, P., O'Neill, B., Blake, A., White, M., Kelleher, A. M., McCarthy, B., and Murphy, R.

Nanowire Transistors without Junctions. *Nature Nanotechnology*, 5, pages 225–229, 2010

[16] Colinge, J. P. Junctionless Transistors. In *IEEE International Meeting for Future of Electron Devices*, pages 1-2, Kansai (IMFEDK), 2012

[17] Colinge, J. P., Kranti, A., Yan, R., Lee, C. W., Ferain, I., Yu, R., Akhavan, N. D., and Razavi P. Junctionless Nanowire Transistor (JNT): Properties and Design Guidelines. *Solid- State Electronics*, 65–66, pages 33-37, 2011

[18] Park, C. H., Ko, M. D., Kim, K. H., Baek, R. H., Sohn, C. W., Baek, C. K., Park, S., Deen, M. J., Jeong, Y. H., and Lee, J. S. Electrical Characteristics of 20-nm Junctionless Si Nanowire Transistors. *Solid-State Electronics*, 73, pages 7–10, 2012

[19] Gnudi, A., Reggiani, S., Gnani, E. and Baccarani, G. Analysis of Threshold Voltage Variability Due to Random Dopant Fluctuations in Junctionless FETs. *IEEE Electron Device Letters*, 33(3), pages. 336–338, 2012.

[20] Lou, H., Zhang, L., Zhu, Y., Lin, X., Yang, S., He, J., and Chan M. A Junctionless Nanowire Transistor with A Dual-material Gate. *IEEE Transactions on Electron Devices*, 59(7), pages 1829–1836, 2012.

[21] Duarte J. P., Kim M. S., Choi S. J. and Choi Y. K. A Compact Model of Quantum Electron Density at The Subthreshold Region for Double-gate Junctionless Transistors. *IEEE Transactions on Electron Devices*, 59(4), pages 1008–1012, 2012.

[22] Gnudi, A., Reggiani, S., Gnani, E. and Baccarani, G. Semi analytical Model of the Subthreshold Current in Short-Channel Junctionless Symmetric Double-Gate Field-Effect Transistors. *IEEE Transactions on Electron Devices*, 60(4), 2013

[23] Li, C., Zhuang, Y., Di, S., and Han, R. Subthreshold Behaviour Models for Nanoscale, Short-Channel Junctionless Cylindrical Surrounding-Gate MOSFETs. *IEEE Transactions on Electron Devices*, 60(11), pages 3655-3662, 2013

[24] Holtij, T., Schwarz, T., Kloes, A., and Iñiguez, B. 2D Analytical Potential Modelling of Junctionless DG MOSFETs in Subthreshold Region Including Proposal for Calculating the Threshold Voltage. In *13th International Conference on ULIS*, pages 81-84, MINATEC Grenoble, France, 2012

[25] Chiang, T. K., A New Subthreshold Current Model for Junctionless Tri-gate MOSFETs to Examine Interface Trapped Charge Effects. *IEEE Transactions on Electron Devices*, 62 (9), pages 2745–2750, 2015

[26] Chiang, T. K., A Quasi-two-dimensional Threshold Voltage Model for Short-Channel Junctionless Double-gate MOSFETs. *IEEE Transactions on Electron Devices*, 59 (9), pages 2284–2289, 2012

[27] Chiang, T. K., A New Quasi-2-D Threshold Voltage Model for Short Channel Junctionless Cylindrical Surrounding Gate (JLCSG) MOSFETs. *IEEE Transactions on Electron Devices*, 59(11), pages 3127–3129, 2012

[28] Trevisoli, R. D., Doria, R. T., de Souza, M., Das, S., Ferain, I., and Pavanello, M. A. Surface Potential Based Drain Current Analytical Model for Triple Gate Junctionless Nanowire Transistors. *IEEE Transactions on Electron Devices*, 59(11), pages 3510–3518, 2012

[29] Barik, M. A., Sarma. M. K., and Dutta, J. C. Surface Potential Based Drain Current Analytical Model for Triple Gate Junctionless Nanowire Transistors. In *IEEE 2nd International Conference on Emerging Electronics (ICEE)*, pages 1-4, IISc, Bangalore, 2014

[30] Barik, M. A., Deka, R., and Dutta, J. C. Carbon Nanotube- Based Dual Gated Junctionless Field-Effect Transistor for Acetylcholine Detection. *IEEE Sensor Journal*, 16(2), pages 280-286, 2016

[31] Colinge, J. P. and Colinge, C. A. *Physics of Semiconductor Devices*, Kluwer Academic Publishers, 2011

[32] Gerald, T. *Ordinary Differential Equations and Dynamical Systems*, American Mathematical Society, 2011